

STELLAR ENCOUNTERS INVOLVING RED GIANTS IN GLOBULAR CLUSTER CORES

M. B. DAVIES AND W. BENZ

Harvard-Smithsonian Center for Astrophysics, 60 Garden Street, Cambridge, MA 02138

AND

J. G. HILLS

Theoretical Division, T-6, MS B288, Los Alamos National Laboratory, Los Alamos, NM 87545

Received 1991 January 14; accepted 1991 May 20

ABSTRACT

Collisions between a $0.8 M_{\odot}$ red giant and impactors of mass 0.4 and $0.6 M_{\odot}$ are simulated using a three-dimensional smoothed particle hydrodynamics (SPH) code. The red giant is modeled as a massive core surrounded by a gaseous envelope, while the impactor, assumed to be a white dwarf or a main-sequence star, is treated as single particle. Encounters at various impact parameters and with relative velocities pertinent to globular clusters (10 km s^{-1}) are studied.

The effect of the encounter on the red giant depends strongly on the impact parameter. We find that if the impactor passes within twice the radius of the red giant ($2R_{\text{RG}}$), mass loss occurs from the red giant envelope and both objects are left bound in elliptical orbits. Calculations suggest that if the impactor has an initial distance at closest approach of approximately $1.6R_{\text{RG}}$ or less, the impactor will spiral in to the red giant envelope on subsequent periastron passages. For bound systems with a greater separation, the orbit may circularize with a radius approximately double that of the initial encounter. In both cases the system will undergo a *common envelope phase*: in the latter case the red giant will eventually fill its Roche lobe as it expands up the giant branch. In the case of a sufficiently small closest approach ($R_{\text{min}} < R_{\text{RG}}$), the impactor is immediately captured by the core of the red giant. Both objects form a binary system orbiting inside a common envelope formed from the original envelope of the giant. Acting like an “eggbeater,” the system spins up the surrounding gas, leading to further mass loss while spiraling together. With a white dwarf impactor, the likely outcome of the common envelope phase will be a tight white dwarf/white dwarf binary that will merge in less than a Hubble time. In the case of a main-sequence star impactor, a tight binary comprised of the main-sequence star and a white dwarf (the red giant core) is likely to be produced, with the main-sequence star filling its Roche lobe.

Subject headings: clusters: globular — stars: late-type — stars: stellar dynamics

1. INTRODUCTION

Stellar collisions are important in galactic nuclei and in the cores of globular clusters. Up to 40% of the stars in some globular cluster cores have suffered physical collisions (Hills & Day 1976). Stellar collisions may even be more important in galactic nuclei. It has been suggested that the gas released could settle to the center of the galactic nucleus to form new stars, ultimately forming a supermassive object at the center (Begelman & Rees 1978). The mass lost from colliding stars in galactic nuclei may provide part of the fuel to power Seyfert galaxies and active galactic nuclei, together with stellar winds and stellar disruptions. Recent models of the evolution of Seyfert galaxies show that at early times stellar winds provide most of the mass to the black hole that grows at an Eddington-limited rate. At later times, however, stellar collisions dominate completely over all other processes as a fuel source to the central engine (Hills 1975, 1978). The study of collisions between red giants and main-sequence stars is also useful in understanding the evolution of common envelope binaries. In these systems the primary has overfilled its Roche lobe and engulfs the secondary with its gaseous envelope. The interaction between the main-sequence star and the common envelope of the contact binary will be similar to that between the outer parts of a red giant and an impacting main-sequence star.

Benz and Hills have already published detailed computa-

tions of collisions between equal-mass main-sequence stars (Benz & Hills 1987) and between white dwarfs (Benz, Hills, & Thielemann 1989) using the smoothed particle hydrodynamics (SPH) method of computational hydrodynamics. We extend this work by simulating encounters between red giants and main-sequence stars, and between red giants and white dwarfs, particularly with masses and impact speeds pertinent to globular clusters. Such collisions are of particular importance because a large fraction of the stars in a globular cluster are low-mass main-sequence stars or low-mass white dwarfs, and red giants have a relatively large collisional cross section. The relative frequency of collisions between different types of stars is examined more quantitatively in § 2. Unlike the collisions previously simulated by Benz and Hills, the collisions we consider are between two objects of very different sizes. It is therefore necessary for numerical reasons to treat the two objects differently. We treat the main-sequence star or white dwarf as a point mass and model the red giant with a massive core (again modeled as a point mass) surrounded by a gaseous envelope having a density distribution based on a stellar model found in the literature. Although some simulations have been done elsewhere (Livne & Tuchman 1988; Rasio & Shapiro 1990, 1991; Goodman & Hernquist 1991), this is the first time that collisions between red giants and main-sequence stars and red giants and white dwarfs are modeled in such a manner. Livne and Tuchman considered encounters involving a *supergiant*

with a radius an order of magnitude larger than the one we consider, and Rasio and Shapiro consider encounters between a red giant and a neutron star.

The work of Livne and Tuchman suggests that the result of a main-sequence star colliding with a red giant depends very strongly on the impact parameter. At high impact parameters, i.e., a grazing collision, slight disruption of the gaseous envelope occurs, but the main-sequence star passes through an otherwise intact red giant. At intermediate impact parameters, more disruption of the envelope occurs, resulting in mass loss from the red giant. At very low impact parameters, the core of the red giant itself is affected by the collision. We therefore study the various consequences of the collisions and how they depend on the initial impact parameter of the main-sequence star or white dwarf.

We present results of encounters between a $0.8 M_{\odot}$ red giant of radius $R_{\text{RG}} = 20 R_{\odot}$ and point masses of mass 0.4 and $0.6 M_{\odot}$. The distance of closest approach ranges between $0.5R_{\text{RG}}$ and $2.5R_{\text{RG}}$. For each encounter, the amount of material escaping from the system is computed together with the amount of material captured by the impactor. We also calculate the shift in the relative velocity of the two objects at infinity and compare this with a simple analytical expression (Bailyn 1988). The subsequent evolution of the system is considered, calculating the time lapse before the second close encounter together with the separation at the second periastron passage. The spin-up of the remains of the red giant is calculated. We also consider the fate of the material that becomes bound to the impactor.

We discuss the subsequent evolution of binary systems that are formed in the encounters. We investigate whether any of the bound systems produced by an initial encounter will circularize rather than have the impactor merely spiral in to the red giant envelope. Even if systems do circularize, the subsequent red giant evolution will result in a common envelope phase. We consider the likely outcome of such a phase in § 5.

2. COLLISION RATES IN GLOBULAR CLUSTER CORES

In this section we quantify the statement made in the introduction that collisions involving red giants are important in globular clusters. For a system where stars of mass m_* have a mean squared velocity dispersion of $\langle v_*^2 \rangle$, the collision rate per unit volume between two stellar species is given by

$$\frac{dn}{dt} = n_1 n_2 \Gamma_{12}, \quad (1)$$

where n_1 and n_2 are the space densities of the two species. In the limit where $v_* \ll V_{\text{esc}}$, the coefficient Γ_{12} is given by (Bailyn, Grindlay, & Garcia 1990)

$$\Gamma_{12} = \langle \sigma V \rangle = \pi(R_1 + R_2)^2 \times \left\{ \left(\frac{3}{\pi} \right)^{1/2} \left(\frac{V_{\text{esc}}^2}{\langle v_*^2 \rangle^{1/2}} \right) \left[\frac{m_1 m_2}{m_*(m_1 + m_2)} \right]^{1/2} \right\}, \quad (2)$$

where m_1 and m_2 are the masses and R_1 and R_2 the radii of the two stars, and V_{esc} is the escape speed between m_1 and m_2 when in physical contact. We are assuming an equipartition of kinetic energy.

Thus, starting with some initial population of stars and using models for the temporal evolution of their radii, it is possible to evolve such a system. In globular clusters we have the added beneficial feature that we can assume that there is

only one era of star formation with ejecta from winds and supernovae being lost from the system. To model the evolution of a globular cluster completely, it is necessary to allow for the mass loss resulting from collisions. It is also important to consider the large-scale dynamical evolution of the cluster. Mass segregation will occur, resulting in an increase in the relative population of the more massive stars in the cluster core. However, by considering a simpler case where we have a uniform isotropic spherical distribution of stars and where all collisions result in mergers, we can at least obtain some reasonable estimates for the collision rates between various types of stars.

We consider 10^5 stars contained within 1 pc^3 . Initially the population follows a power law similar to the Salpeter mass function. We assume that no later star formation occurs after the initial creation of this population. Using equation (2) to calculate the rate coefficients between the various stellar species, together with equation (1), the system of stars is evolved using the models for stellar evolution produced by Mengel, Sweigart, & Demarque (1979) to calculate time-averaged radii for the main-sequence and red giant stars of various masses. As a simplifying assumption, we do not allow the products of mergers to undergo any further collisions. This results in only a small error, as the fraction of stars involved in encounters is small. We find that main-sequence/main-sequence collisions are the most common, and we have approximately one-fourth as many involving red giants with end states or main-sequence stars. The number changes only slightly with the slope of the IMF or the lowest mass assumed. These are the second most important collisions.

3. NUMERICAL METHOD AND INITIAL CONDITIONS

The simulations were produced using a three-dimensional smoothed particle hydrodynamics (SPH) code. For further discussion of SPH see Benz (1990). All the collisions involved a $0.8 M_{\odot}$ red giant constructed using 7132 SPH particles of variable smoothing length and a point-mass core. We use a realistic equation of state for the gas in the red giant envelope, including both radiation and gas pressure:

$$P = \frac{\rho RT}{\mu} + \frac{\alpha T^4}{3}. \quad (3)$$

A red giant has a density distribution more centrally peaked than a main-sequence star. If the red giant were modeled with 10,000 equally spaced particles, the average particle spacing, and the smoothing length h , would be of the order of $0.1R_{\text{RG}}$. Approximately 40% of the mass of the red giant is enclosed within a radius of $0.1R_{\text{RG}}$. Hence in this case the central particle would account for the order of 40% of the star's total mass! There is no reason why all the particles *must* have the same mass, though a broad range of masses may lead to problems when mixing occurs in a collision. Further, since SPH uses interpolation to calculate physical quantities such as density, the *extremely* high values at the center will be interpolated out to $2h$, i.e., $0.2R_{\text{RG}}$. This will result in a severe broadening of the central density and pressure peaks. The above problems can be avoided by substituting a point mass for the SPH particle at the center of the red giant. Such a point mass interacts with the SPH particles via the gravitational force (with a short-range repulsive force to avoid SPH particles coming infinitely close). The gaseous envelope of the star is modeled with SPH particles.

Similarly, an $0.6 M_{\odot}$ main-sequence star, which has a radius of $0.6 R_{\odot}$ or $0.03 R_{\text{RG}}$, is actually smaller than the mean interparticle distance. Furthermore, because of the extremely large density difference between the giant's envelope and the main-sequence star, the latter will not be affected by passing through the giant's envelope. Hence, we approximate the intruder by a point mass as well. Obviously, the above argument is even more true for a white dwarf.

3.1. Producing the Red Giant

The envelope density distribution is determined by solving numerically the hydrostatic equilibrium equation, taking into account the presence of a point-mass core. Using the evolutionary model for an $0.8 M_{\odot}$ star given by McMillan, Taam, & McDermott (1990), we chose a core mass of $0.32 M_{\odot}$ for the giant corresponding to a star in the middle of the giant branch. Finally, the entropy is chosen so that we obtain a red giant radius $R_{\text{RG}} = 1.3683 \times 10^{12}$ cm as required by the above model.

4. RESULTS

In the first group of collisions listed in Table 1, the mass ratio between the point-mass impactor and the red giant is $q = 0.5$, i.e., $M_{\text{imp}} = 0.4 M_{\odot}$. Such a ratio is applicable when the impactor being considered is a main-sequence star. For the other collisions listed, $q = 0.75$, or, equivalently, $M_{\text{imp}} = 0.6 M_{\odot}$, a typical mass for a white dwarf. In all collisions we set $v_{\infty} = 10 \text{ km s}^{-1}$. With the exception of the two encounters with the closest initial impact parameters, only the first approach between the red giant and the point-mass impactor is simulated; for those cases where a bound binary forms, the time to the second approach (periastron passage) would make the simulation run times prohibitively long.

A series of snapshots of a typical encounter is given in Figure 1. In this encounter, $q = 0.75$, and the distance of closest approach of the *initial* encounter divided by the red giant radius is $x_0 = R_{\text{min}}/R_{\text{RG}} = 1.25$. We see that material is shed from the outer layers of the envelope of the red giant as the point mass passes by. Some of this material is lost from the system, and some becomes bound to the impactor. After their initial encounter, the impactor, together with its accreted gas,

TABLE 1
RESULTS OF FIRST ENCOUNTERS

| Collision | $x_0 (R_{\text{min}}/R_{\text{RG}})$ | $M_{\text{acc}}/M_{\text{env}}$ | $M_{\text{lost}}/M_{\text{env}}$ | $(\delta v_{\infty}^2)^{1/2}$ (km s^{-1}) |
|-----------------|--------------------------------------|---------------------------------|----------------------------------|---|
| ColLA.10a | 2.25 | 0 | 0 | 4.4 |
| ColLA.4a | 2.0 | 3.522E - 4 | 0 | 8.19 |
| ColLA.6a | 1.75 | 3.712E - 4 | 4.72E - 4 | 14.30 |
| ColLA.5a | 1.5 | 4.415E - 3 | 1.21E - 3 | 22.98 |
| ColLA.7a | 1.25 | 1.145E - 2 | 3.58E - 3 | 32.7 |
| ColLA.8a | 1.0 | 1.98E - 2 | 1.09E - 2 | 44.6 |
| ColLA.9a | 0.75 | 2.435E - 2 | 2.77E - 2 | 61.2 |
| ColLA.11a | 0.5 | 5.946E - 2 | 5.77E - 2 | 92.1 |
| ColLA.5b | 2.5 | 0 | 0 | 0.75 |
| ColLA.9b | 2.25 | 0 | 0 | 7.05 |
| ColLA.1b | 2.0 | 1.57E - 4 | 7.10E - 4 | 12.18 |
| ColLA.6b | 1.75 | 6.90E - 3 | 1.27E - 3 | 19.81 |
| ColLA.2b | 1.5 | 1.47E - 2 | 2.90E - 3 | 28.58 |
| ColLA.7b | 1.25 | 2.75E - 2 | 8.29E - 3 | 38.47 |
| ColLA.3b | 1.0 | 4.92E - 2 | 1.78E - 2 | 50.74 |
| ColLA.8b | 0.75 | 6.45E - 2 | 4.40E - 2 | 67.31 |
| ColLA.4b | 0.5 | 9.43E - 2 | 8.34E - 2 | 98.96 |

and the remains of the red giant are left bound in eccentric orbits. The fractional mass of the envelope of the red giant accreted and lost for this and all other collisions is given in Table 1. Originally the mass of the gaseous envelope M_{env} was $0.48 M_{\odot}$. In the two cases where $x_0 = 0.5$, we calculate the values in Table 1 when the point mass is midway between the first and second closest approaches.

The various energies of the system for this encounter are illustrated in Figure 2. Total energy is conserved to $\sim 0.1\%$ or less, and angular momentum is conserved to $\sim 0.03\%$ or less. Note that we do not show the energies of the escaping gas and those of the mass transferred to the compact object separately, as these contributions are small compared with those from the material remaining in the red giant envelope (fractions of thermal and kinetic energies of the gas not contained in the red giant envelope are $\lesssim 1\%$ and $\lesssim 25\%$, respectively). The main source for the change in orbital energy is the energy dissipated within the red giant envelope, mostly in heating it up but also in spinning up the star. The energy carried off by the mass lost from the system is small by comparison.

After the first approach, and by treating the remains of the red giant and the point-mass impactor, with its captured material, as a two-body system, we calculate the energy dissipated and obtain a new value for v_{∞}^2 . This assumption is justified, since at the end of the run the red giant core and the impactor are more than $9R_{\text{RG}}$ apart. By subtracting the original v_{∞}^2 , we calculate $(\delta v_{\infty}^2)^{1/2}$. The values obtained for the various encounters are given in Table 1. For the system to become bound, we need at least $(\delta v_{\infty}^2)^{1/2} \gtrsim 10 \text{ km s}^{-1}$. Hence we see that x_{crit} , the value of x for which the system is just bound, is approximately 2.0 for both values of q .

4.1. Mass Loss

The mass fraction of the red giant envelope lost is plotted in Figure 3 as a function of x_0 for both values of q . We see that mass loss increases with q and decreases with x_0 , as would be expected. The mass-loss cross section is given by

$$\sigma = \int_0^{\infty} 2\pi AP dP, \quad (4)$$

where A is the fractional mass loss in the encounter, $A = M_{\text{lost}}/(M_{\text{RG}} + M_{\text{imp}})$, and P is the impact parameter. Following the method of Benz & Hills (1987), we can calculate the mass-loss cross section divided by the geometrical cross section. Using the numerical values of A as a function of R_{min} derived from Table 1, we obtain

$$\frac{\sigma}{\pi(R_{\text{RG}} + R_{\text{imp}})^2} = \begin{cases} 0.05(V_{\text{esc}}/V)^2 & \text{for } q = 0.5, \\ 0.05(V_{\text{esc}}/V)^2 & \text{for } q = 0.75. \end{cases} \quad (5)$$

It is interesting to note the independence of this value of q ; also, it should be noted that this value is $\simeq 3$ times larger than that obtained for collisions between equal-mass main-sequence stars (Benz & Hills 1987).

4.2. Tidal Dissipation and Scaling Laws

The tidal oblateness ϵ of a star of mass M_{RG} caused by a passing star of mass M_{imp} is approximately $\epsilon \simeq f M_{\text{imp}} x^{-3}/M_{\text{RG}}$, where $x = d/R_1$, d is the distance between the two stars, and f is a constant less than or equal to 1 (Fabian, Pringle, & Rees 1975; Baily 1988). The energy associated with such a tidal bulge is $E_{\text{tidal}} \simeq (Gm_{\text{RG}} M_{\text{env}}/R_{\text{RG}})\epsilon^2$, where M_{env} is the mass of the envelope of the deformed star. Hence, in the

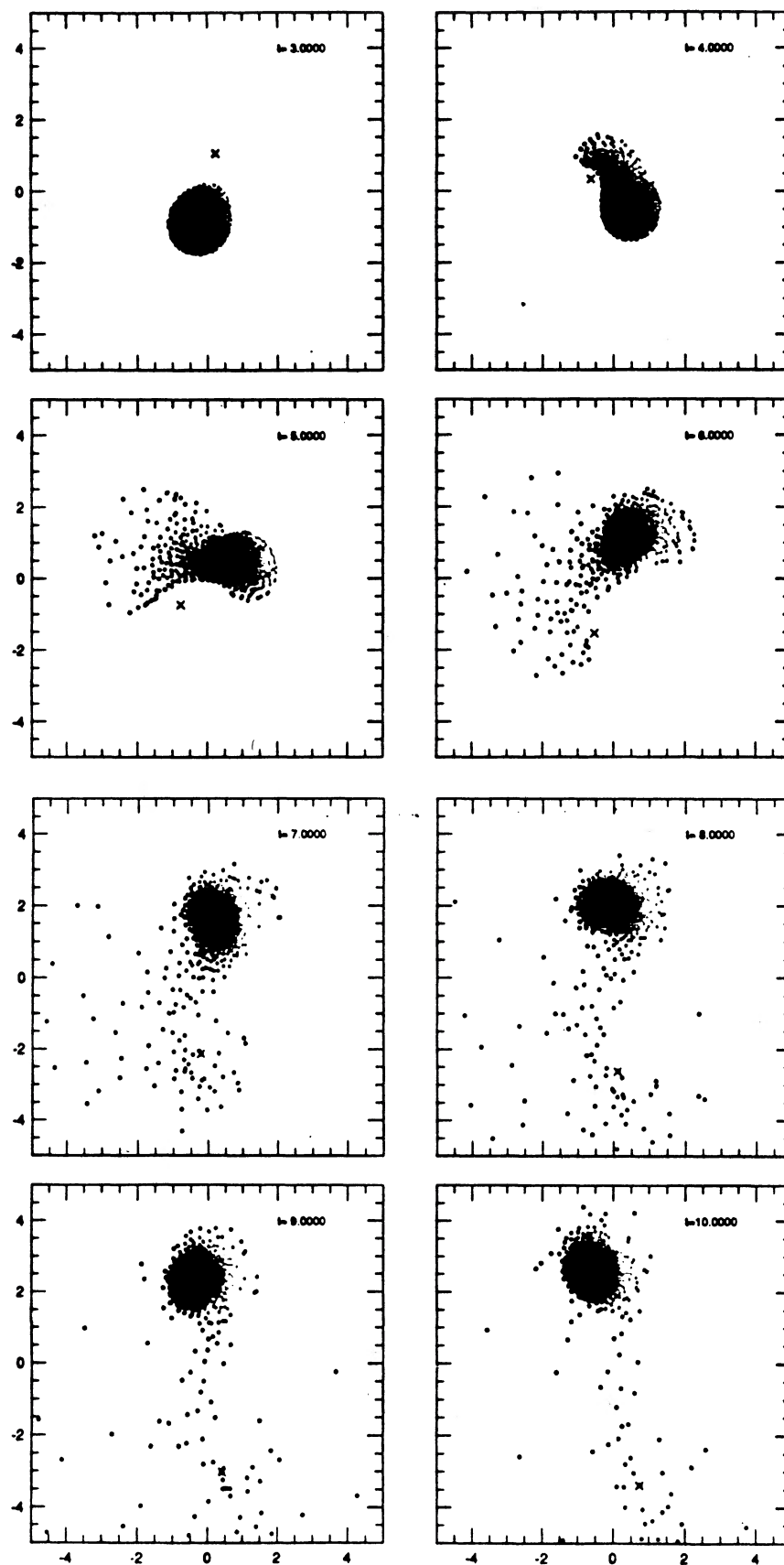


FIG. 1.—Snapshots of the simulation CollA.7b, with $x_0 = 1.25$ and $M_{\text{imp}} = 0.6 M_{\odot}$ (1 time unit \equiv 2.3 days)

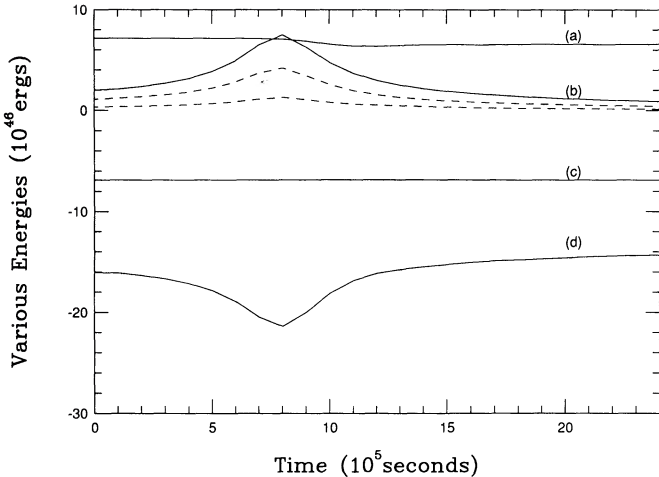


FIG. 2.—Various energies of the system for the encounter illustrated in Fig. 1: (a) the thermal energy of the gas, (b) the total kinetic energy, (c) the total energy, and (d) the potential energy. The two dotted lines are the kinetic energies of the red giant core and the impactor, the latter having the larger value.

case of the red giant–impactor system, the expected tidal energy is given by

$$E_{\text{tidal}} = \left(\frac{GM_{\text{RG}} M_{\text{env}}}{R_{\text{RG}}} \right) f^2 \frac{M_{\text{imp}}^2}{M_{\text{RG}}^2 x_0^6}, \quad (6)$$

where M_{RG} and M_{imp} are the masses of the red giant and impactor, and R_{RG} is the radius of the red giant. Since the tidal energy equals the change on orbital kinetic energy, we have

$$(\delta v_{\infty}^2)^{1/2} \propto \frac{[q(1+q)]^{1/2}}{x^3}. \quad (7)$$

We expect this behavior of $(\delta v_{\infty}^2)^{1/2}$ for x_0 somewhat larger than unity where the approximations made in obtaining equation (6) are more justified. The orbital velocity change at infinity, $(\delta v_{\infty}^2)^{1/2}$, is plotted in Figure 4 against the distance of closest approach, x_0 , for both values of q . We see that both curves approach the dependence on x predicted by the above

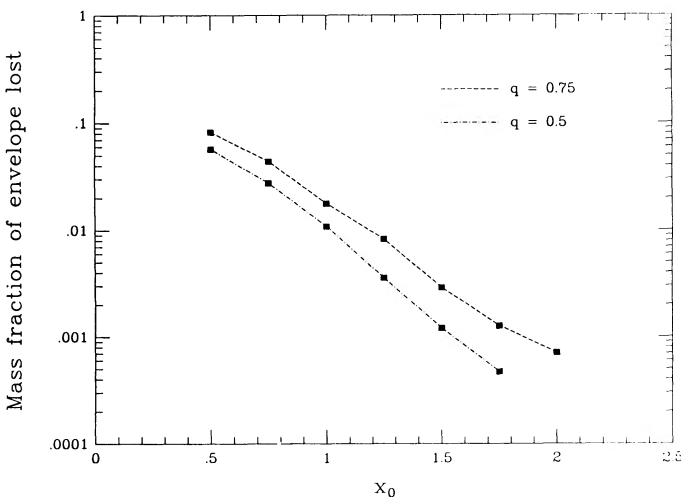


FIG. 3.—Mass fraction of the envelope lost after the first encounter as a function of the distance at closest approach, x_0 (in units of red giant radius R_{RG}).

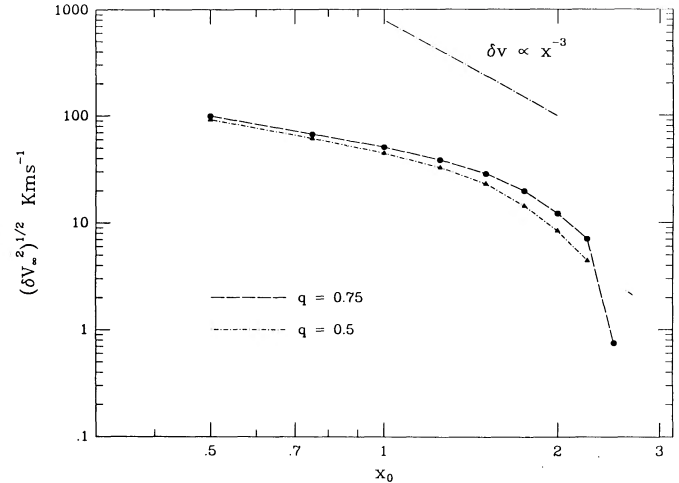


FIG. 4.—Velocity change at infinity, $(\delta v_{\infty}^2)^{1/2}$, as a function of the distance at closest approach, x_0 (in units of red giant radius R_{RG}).

equation for $1.5 < x_0 < 2.0$. For smaller values of x_0 , the tides raised are in the nonlinear regime. It should also be noted that small values of $(\delta v_{\infty}^2)^{1/2}$ are accompanied by larger fractional errors, since the error in the total energy conservation of the system is equivalent to an uncertainty in the relative velocity of $\approx 1 \text{ km s}^{-1}$.

We calculate the ratio between the velocity shifts for the two values of q for the various values of x_0 . We find that the mean of the ratios is 1.3, which agrees very well with the value of 1.32 predicted by equation (7).

4.3. The Fate of the Red Giant

Initially the red giant is not rotating. After the first encounter with the point mass it is given a “kick.” Below we discuss the observational effects of this angular momentum transfer and whether the red giant will be spun up sufficiently for rotational instabilities to become important.

We look at the particles that remain bound to the red giant core at the end of the first encounter. By working in the rest frame of the red giant core, we calculate the angular momentum contained in the postencounter star. The convective friction time scale for the red giant, i.e., the time for the star to become a rigid rotator, is given by (Zahn 1989)

$$t_f = 0.433 \left[\left(\frac{M}{M_{\odot}} \right) \left(\frac{R}{R_{\odot}} \right)^2 \left(\frac{L_{\odot}}{L} \right) \right]^{1/3} \text{ yr}. \quad (8)$$

For the red giant considered here, $M = 0.8 M_{\odot}$, $R = 20 R_{\odot}$, and the luminosity L is $150 L_{\odot}$. Hence $t_f \approx 0.6 \text{ yr}$. It is therefore reasonable to estimate the rotation rate of the red giant, Ω_{RG} , by assuming rigid rotation, i.e., by dividing the angular momentum contained in the star by the moment of inertia. We find that $\Omega_{\text{RG}} \lesssim 3 \times 10^{-6} \text{ radians s}^{-1}$, corresponding to a rotation period $\approx 24 \text{ days}$.

The ratio of the rotational to the absolute value of the gravitational potential energy, $\beta = T/|W|$, is a well-known indicator of rotational instabilities. The classical global dynamical instability occurs for $\beta = 0.2738$ in the case of Maclaurin spheroids. This critical value for β , derived for incompressible, homogeneous fluids, has been shown to hold also for polytropic configurations (Durisen & Tohline 1985). However, in the case of centrally condensed objects the critical value for β may never be reached by progressive spin-up. Indeed, once the

equatorial velocity reaches the Keplerian value, any further increase will result in mass shedding from the equator. For rigidly rotating objects of constant density, the critical value of β for mass shedding is $\frac{1}{3}$ whereas for a uniformly rotating polytrope of index $n = 3$ this critical value is 0.025 (Shapiro & Teukolsky 1983). Centrally condensed objects in uniform rotation are subject to mass shedding at lower values of β than objects of uniform density. In the case of our red giant, the critical value is 0.022. The maximum value of β after any first encounter is ≈ 0.005 . In confirmation of this calculation, we do not see any mass shedding at the end of any of our simulations.

4.4. The Fate of the Gas Accreting onto the Impactor

Working in the rest frame of the compact object, we calculate the angular momentum contained in the SPH particles bound to the point mass. Assuming that these particles maintain their individual angular momentum, we can calculate the radius of an equivalent Keplerian circular orbit. A disk of material would possibly form around the impactor if it were unaffected by the subsequent evolution of the system. The radius of this disk appears to be highly dependent on the value of x_0 but will be $\approx 10\text{--}40 R_\odot$. However, such a disk will be disrupted on the second periastron passage of the impactor around the red giant, as the impactor will typically pass within $\approx 10\text{--}20 R_\odot$ of the red giant surface.

4.5. Evolution after the First Encounter

As stated above, the grazing collisions leave the red giant and the impactor in eccentric orbits. Treating the remains of the red giant and the impactor (together with the material bound to it) as a two-body system, we calculate the time elapsed before a second close approach, τ_{ret} , together with the closest approach at this second encounter, x_1 . These values together with the closest approach for the first encounter are given in Table 2. We see that the time before a second encounter depends strongly on the initial distance of closest approach. For $1.0 < x_0 < 2.0$, a second encounter will occur $\approx 10^2\text{--}10^4$ days later. Two competing effects determine the minimum distance between the two objects on subsequent encounters. Every encounter results in the transfer of orbital angular momentum into the rotational angular momentum of the

TABLE 2
DETAILS OF CALCULATED SECOND ENCOUNTERS

| Collision | x_0 | x_1 | τ_{ret} (days) |
|-----------|-------|----------------------|-------------------------------|
| ColLA.10a | 2.25 | Unbound | ∞ |
| ColLA.4a | 2.0 | Unbound | ∞ |
| ColLA.6a | 1.75 | 1.748 | 4690.7 |
| ColLA.5a | 1.5 | 1.486 | 570.4 |
| ColLA.7a | 1.25 | 1.212 | 169.8 |
| ColLA.8a | 1.0 | 0.927 | 64.8 |
| ColLA.9a | 0.75 | 0.6753 | 26.5 |
| ColLA.11a | 0.5 | Tightly bound system | |
| ColLA.5b | 2.5 | Unbound | ∞ |
| ColLA.9b | 2.25 | Unbound | ∞ |
| ColLA.1b | 2.0 | 1.9985 | 18009.3 |
| ColLA.6b | 1.75 | 1.7426 | 1172.0 |
| ColLA.2b | 1.5 | 1.470 | 310.4 |
| ColLA.7b | 1.25 | 1.192 | 117.6 |
| ColLA.3b | 1.0 | 0.900 | 51.6 |
| ColLA.8b | 0.75 | 0.631 | 23.6 |
| ColLA.4b | 0.5 | Tightly bound system | |

TABLE 3
SPIN-UP OF RED GIANT

| Collision | x_0 | $\Omega_{\text{RG}}/\Omega_{\text{Kep}}$ | $\Omega_{\text{orb}}/\Omega_{\text{Kep}}$ |
|-----------|-------|--|---|
| ColLA.10a | 2.25 | 0.006 | 0.398 |
| ColLA.4a | 2.0 | 0.020 | 0.474 |
| ColLA.6a | 1.75 | 0.055 | 0.580 |
| ColLA.5a | 1.5 | 0.115 | 0.730 |
| ColLA.7a | 1.25 | 0.197 | 0.960 |
| ColLA.8a | 1.0 | 0.252 | 1.342 |
| ColLA.9a | 0.75 | 0.259 | 2.066 |
| ColLA.11a | 0.5 | 0.312 | 3.795 |
| ColLA.5b | 2.5 | 0.006 | 0.367 |
| ColLA.9b | 2.25 | 0.021 | 0.429 |
| ColLA.1b | 2.0 | 0.060 | 0.512 |
| ColLA.6b | 1.75 | 0.106 | 0.626 |
| ColLA.2b | 1.5 | 0.218 | 0.789 |
| ColLA.7b | 1.25 | 0.303 | 1.037 |
| ColLA.3b | 1.0 | 0.363 | 1.449 |
| ColLA.8b | 0.75 | 0.410 | 2.231 |
| ColLA.4b | 0.5 | 0.480 | 4.099 |

gaseous envelope of the red giant. It is thus reasonable to expect that, in a bound system, we will have a subsequent series of closer encounters resulting in the eventual merger of the point-mass impactor and the remains of the red giant. We expect spin-up of the red giant to occur until $\Omega_{\text{RG}} \approx \Omega_{\text{orb}}$; where Ω_{RG} is the rotation rate of the red giant and Ω_{orb} is the rotation rate of the point mass around the red giant in its rest frame at the first periastron passage. Table 3 gives Ω_{RG} and Ω_{orb} (renormalized by the Keplerian breakup rotation rate, Ω_{Kep}) after various first encounters. We see that spin-up of the red giant will occur for many subsequent encounters as typically $\Omega_{\text{RG}} \ll \Omega_{\text{orb}}$ after the first encounter. However, circularization of the orbits of the two objects may also occur, which would yield a mean separation $\approx 2x_0$ by conservation of angular momentum. Even if the latter effect dominates, the subsequent evolution of the red giant would cause it to engulf the point mass, forming a *common envelope system* not too dissimilar from that formed in encounters with $x_0 = 0.5$. We will return shortly to a discussion of the subsequent evolution of these systems.

The ratio x_1/x_0 is plotted against x_0 in Figure 5. We see that for both values of q , the value of x_1/x_0 asymptotically tends to unity for large x_0 ; we never see $x_1/x_0 > 1$. Hence it is clear that the effects of circularization are small on all first approaches.

4.5.1. The Properties of a Circularized System

Let us neglect for one moment the theoretical difficulties of calculating the circularization time scale and suppose that such systems can be formed. We can imagine an idealized system where the point mass orbits in a circle around the red giant, whose rotation period matches the orbital period of the point mass and compute the orbital separation R_{orb} of such a system. For a stable circularized system, we must also check that the red giant system is not overflowing its Roche lobe. The equivalent Roche radius of a star in a binary system is given by (Eggleton 1983)

$$r_L(q) = \frac{0.49q^{2/3}}{0.6q^{2/3} + \ln(1 + q^{1/3})}, \quad (9)$$

where, in this case, $q = M_{\text{RG}}/M_{\text{imp}}$. We obtain $r_L = 0.44$ for $M_{\text{imp}} = 0.4 M_\odot$ and $r_L = 0.404$ for $M_{\text{imp}} = 0.6 M_\odot$. The radius

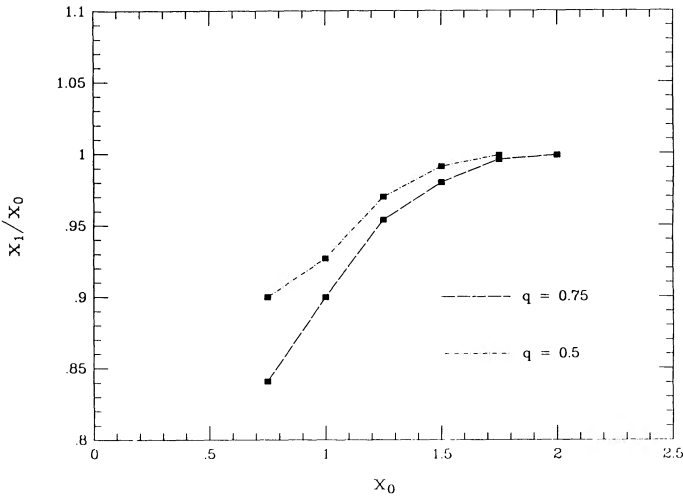


FIG. 5.—Distance at the second periastron passage divided by the distance at the first periastron passage, x_1/x_0 , as a function of x_0 .

of a star filling its Roche lobe is given by $R_L = r_L R$. In Table 4 we give R_{orb}/R_{RG} , R_L/R_{RG} , and the orbital period P_{orb} of circularized systems that could be produced by the various encounters. We thus see that even if we could circularize the orbits, the systems where $x_0 \lesssim 1.25$ cannot form stable circularized systems, as the red giants would overflow their Roche lobes.

4.5.2. Will Any Systems Circularize?

We now consider the question of circularization in more detail. Once the impactor becomes bound to the red giant, it will spin it up on subsequent periastron passages. The orbit of the impactor will begin to circularize once $\Omega_{RG} \approx \Omega_{orb}$. We have to find whether we can achieve this condition before the impactor spirals in to the red giant envelope. To investigate the spin-up of the red giant on subsequent encounters with the impactor, we carried out some encounter simulations, where the initial red giant spin was *nonzero*, $q = 0.75$ and $x_0 = 1.5$. In Figure 6 we plot x_1/x_0 as a function of Ω_{RG} . As expected, we see that $x_1/x_0 \approx 1.0$ when $\Omega_{RG} \approx \Omega_{orb}$. Indeed x_1/x_0 seems to vary linearly with Ω_{RG} . In Figure 7 we plot the change in the rotation rate of the red giant, $\Delta\Omega_{RG}$, after the first encounter as a function of the initial spin. Again, we see a linear variation with Ω_{RG} and $\Delta\Omega_{RG} \approx 0.0$ when $\Omega_{RG} = \Omega_{orb}$. From the simulations carried out with the red giant having zero initial spin, we know how x_1/x_0 and $\Delta\Omega_{RG}$ depend on x_0 when $\Omega_{RG} = 0.0$. If we assume that x_1/x_0 goes linearly from these values to unity and $\Delta\Omega_{RG} \rightarrow 0.0$ as $\Omega_{RG} \rightarrow \Omega_{orb}$, we then have x_1/x_0 and $\Delta\Omega_{RG}$ as a function of *both* x_0 and Ω_{RG} . We are thus able to “evolve”

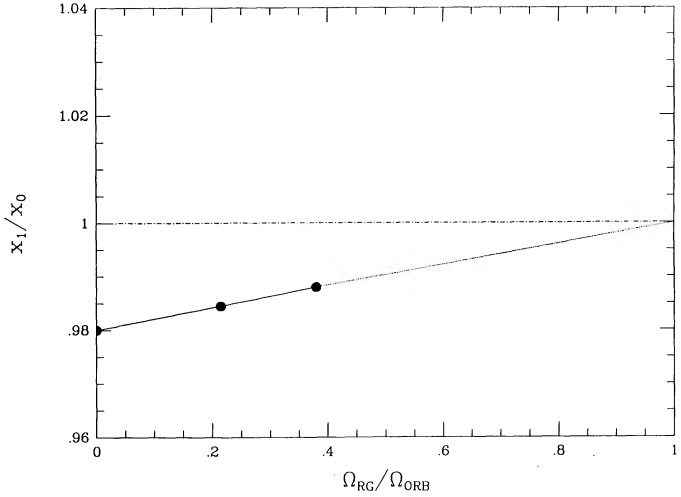


FIG. 6.—Ratio x_1/x_0 as a function of the red giant rotation rate Ω_{RG} for $x_0 = 1.5$ and $M_{imp} = 0.6 M_\odot$.

a system with an initial separation, x_0 , and $\Omega_{RG} = 0.0$ on its subsequent periastron passages. The evolution of Ω_{RG} and Ω_{orb} are illustrated in Figures 8 and 9 for various values of x_0 . We see that the system will circularize when $x_0 \lesssim 1.64$ with $q = 0.75$ and when $x_0 \gtrsim 1.56$ with $q = 0.5$. Hence circularized systems seem the likely product of $\approx 25\%$ of the bound systems produced. Smaller values of x_0 will produce merged systems as either the red giant is spun up until $\Omega_{RG} \approx \Omega_{Kep}$, in which case it will swallow up the impactor as its equatorial radius increases, or the impactor spirals into the envelope as the distance of closest approach on subsequent periastron passages approaches the red giant radius.

At this point, we should mention some of the assumptions made in the above analysis. First, we have assumed that the red giant will be a rigid rotator by the time a second encounter occurs. As discussed earlier, convection within the envelope will lead to rigid rotation in ≈ 0.6 yr. Hence inspection of Table 2 tells us that the red giant will be a rigid rotator at the time of a second encounter for $x_0 \gtrsim 1.5$. It should also be pointed out that the dynamical time scale of the red giant is of

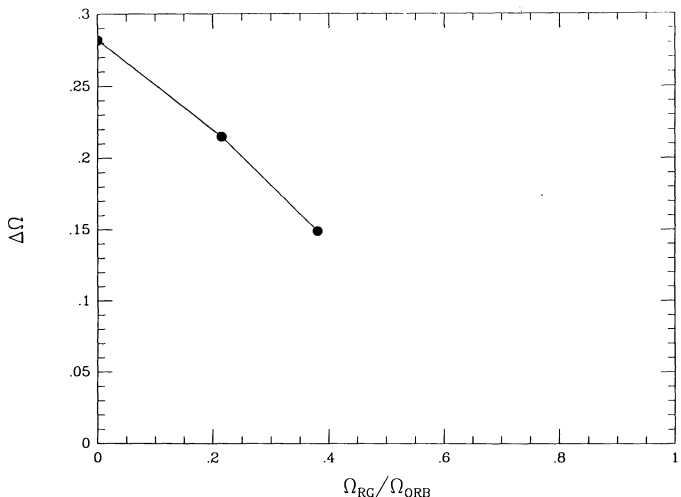


FIG. 7.—Shift in the red-giant rotation rate, $\Delta\Omega_{RG}$, as function of Ω_{RG} for $x_0 = 1.5$ and $M_{imp} = 0.6 M_\odot$.

TABLE 4

PROPERTIES OF CIRCULARIZED SYSTEMS

| Collision | x_0 | R_{orb}/R_{RG} | R_L/R_{RG} | P_{orb} (days) |
|----------------|-------|------------------|--------------|---------------------|
| CoILA.4a | 2.0 | 3.883 | 1.708 | 70.52 |
| CoILA.6a | 1.75 | 3.351 | 1.47 | 56.52 |
| CoILA.5a | 1.5 | 2.808 | 1.23 | 43.38 |
| CoILA.7a | 1.25 | 2.247 | 0.99 | 31.01 |
| CoILA.1b | 2.0 | 3.913 | 1.58 | 66.05 |
| CoILA.6b | 1.75 | 3.3877 | 1.37 | 53.22 |
| CoILA.2b | 1.5 | 2.856 | 1.15 | 41.18 |
| CoILA.7b | 1.25 | 2.31165 | 0.93 | 29.99 |

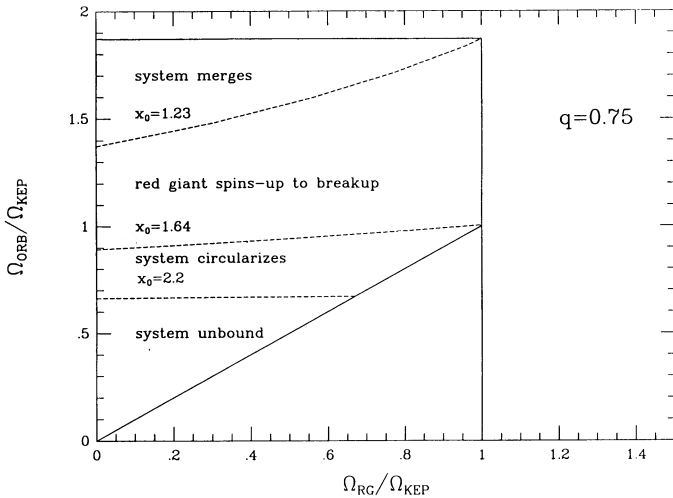


FIG. 8.—Evolution of bound systems, with $M_{\text{imp}} = 0.6 M_{\odot}$, on subsequent periastron passages of the impactor around the red giant.

the order of a few days, whereas the thermal time scale is approximately 7000 yr. The red giant will therefore not have time to reach a thermal equilibrium before the second periastron passage of the impactor. On this second encounter, the red giant envelope will be slightly bloated with a layer of higher entropy material on its surface. There will also be a ring of material around the red giant as well as a disk around the impactor. We expect that the increased radius of the red giant and the presence of the material around both stars will lead to a more rapid spiraling in of the impactor than we have calculated above. Hence the calculated minimum values of x_0 required to produce circularized systems should be taken as *lower limits*.

4.6. The Result of a Close Physical Collision—Common Envelope Systems

A good illustration of a typical collision at a small impact parameter is one with a $0.6 M_{\odot}$ impactor at a distance of closest approach $x_0 = 0.5$. A series of snapshots of this simulation is shown in Figure 10. The second close approach occurs less than 20 days after the initial encounter. A tight binary

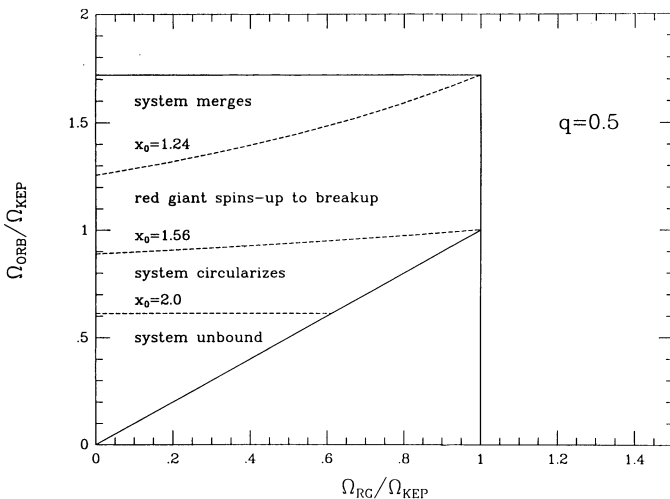


FIG. 9.—As in Fig. 8, but with $M_{\text{imp}} = 0.4 M_{\odot}$.

comprising the impactor and the red giant core then forms with an initial separation of 10^{12} cm ($\approx 15 R_{\odot}$), engulfed in what remains of the red giant envelope. As time goes by, the binary orbits become less eccentric. The angular momentum of the SPH particles (center-of-mass frame) is plotted in Figure 11. This value remains constant (being some fraction of the total orbital angular momentum) until a time of $\approx 6 \times 10^5$ s, when the impactor strikes the red giant. The point-mass impactor then dumps angular momentum into the gaseous envelope. One observes a steady increase in the angular momentum contained in the gas with sporadic peaks corresponding to periastron passages by the impactor about the red giant core. This binary system acts as an “eggbeater,” stirring up the gaseous envelope after the initial ejection of material when the impactor first strikes the envelope of the red giant and resulting in additional mass loss as is illustrated in Figure 12. A density contour map in a plane perpendicular to that of the initial trajectories is shown in Figure 13. One observes that the system has become somewhat flattened by rotation. It is also interesting to note that both the impactor and the red giant core, denoted in this figure by crosses, have similar local gas densities. If the binary fails to eject all of the envelope, a rapidly rotating red giant will remain. One may expect an increase in the surface abundance of metals in such a star, since processed material is likely to be “dredged up” from the center.

Such *common envelope* systems are of interest not only in the study of the effects of close encounters between stars in dense stellar systems but also in understanding how to form white dwarf binaries and cataclysmic variables. As mentioned earlier, *all* binaries formed from the encounters between the impactor and the red giant will pass through a similar phase, even if the binary system circularizes, since the red giant will fill its Roche lobe when it further evolves and expands. A more detailed discussion of the common envelope phase follows in the next section.

5. DISCUSSION

5.1. Common Envelopes Formed in Close Physical Collisions

First we consider the result of the penetration of the red giant envelope by the point mass *before* the system circularizes. The point mass will spiral in toward the core as the envelope is ejected. By considering the energy required to remove the envelope of gas, we can learn something about the ultimate fate of the impactor and the red giant core. The binding energy of the envelope is given by (de Kool 1990)

$$E_{\text{env}} = \frac{G(M_c + M_{\text{env}})M_{\text{env}}}{\lambda R_{\text{RG}}}, \quad (10)$$

where M_{env} is the envelope mass, R_{RG} is the red giant radius, and λ is a numerical factor of order unity that depends on the density distribution of the envelope. Let us suppose that all the envelope is ejected and let the final core–point-mass separation be denoted by a_f . The change in binding energy of the impactor on the onset of the common envelope phase and the removal of the entire envelope is given by

$$\Delta E_g = \frac{GM_{\text{imp}}M_c}{2a_f} - \frac{GM_{\text{imp}}(M_c + M_{\text{env}})}{2a_i}, \quad (11)$$

where a_i is the initial separation of the core and impactor. Thus we can find the final separation of the core and the impactor

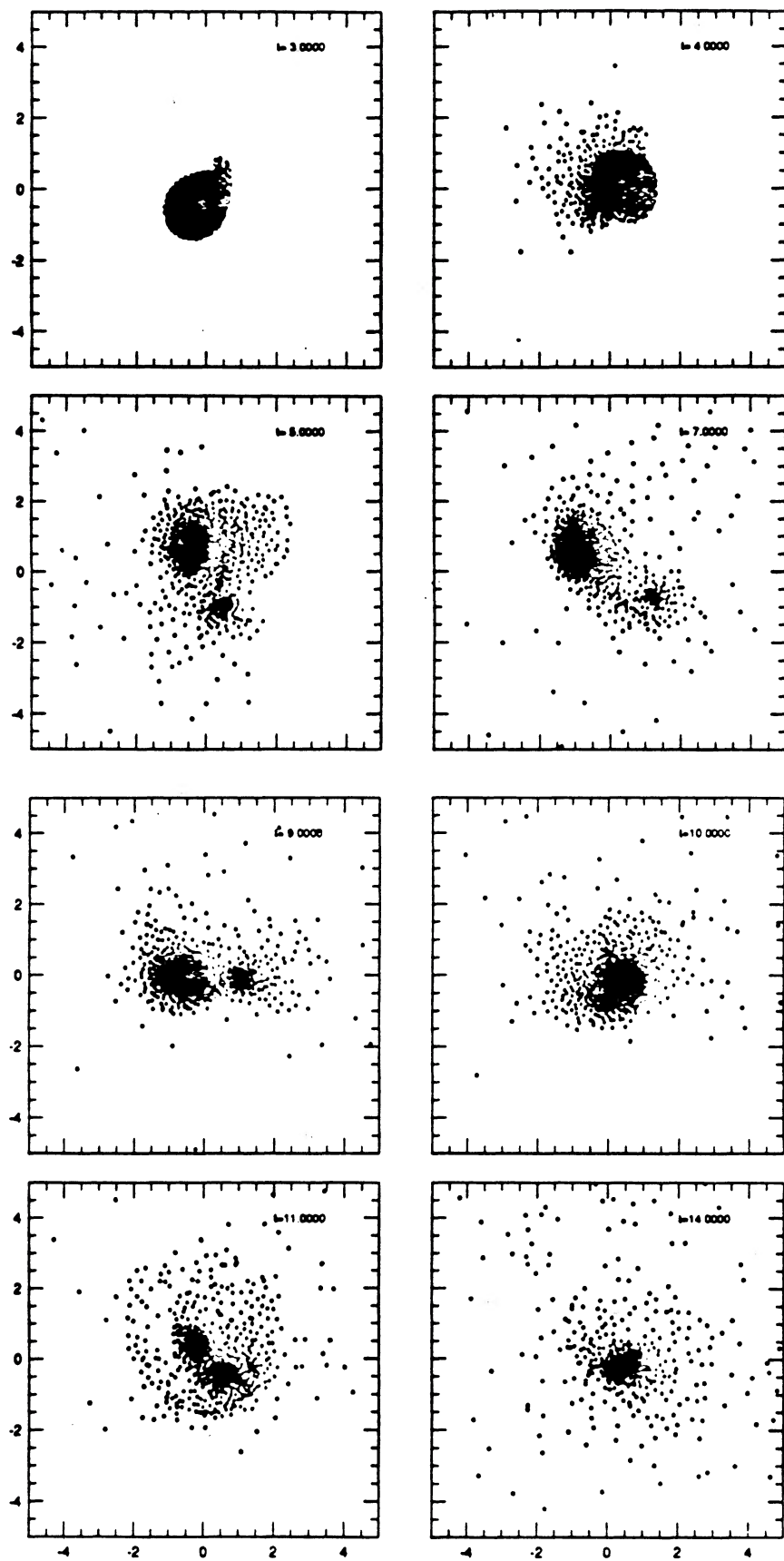


FIG. 10.—Snapshots of the simulation with $M_{\text{imp}} = 0.6 M_{\odot}$ and $x_0 = 0.5$ (1 time unit \equiv 2.3 days)

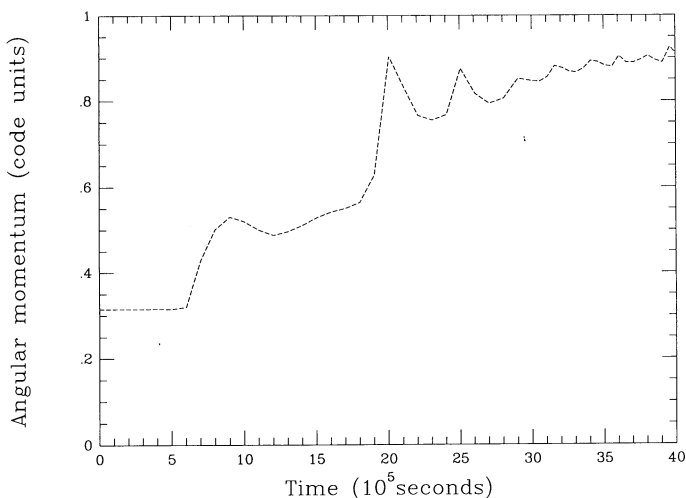


FIG. 11.—Angular momentum of the SPH particles (center-of-mass frame) as a function of time for the simulation illustrated in Fig. 10.

assuming that all of the envelope is removed with an efficiency α , where

$$E_{\text{env}} = \alpha \Delta E_g. \quad (12)$$

Combining the above two equations, we obtain

$$a_f = M_c \left(\frac{2E_{\text{env}}}{G\alpha M_{\text{imp}}} + \frac{M_c + M_{\text{env}}}{a_i} \right)^{-1}. \quad (13)$$

Inserting suitable values in the above equation, we obtain

$$a_f = 13.334 \left(\frac{1.485}{\alpha M_{\text{imp}}} + \frac{33.334}{a_i} \right)^{-1}, \quad (14)$$

where a_i and a_f are given in units of R_\odot , and M_{imp} is in units of M_\odot .

5.1.1. Main-Sequence Impactor

Consider the case of a main-sequence star striking the red giant. The subsequent common envelope phase has three possible results. If the final separation between the main-sequence star and white dwarf (previously the red giant core) is suffi-

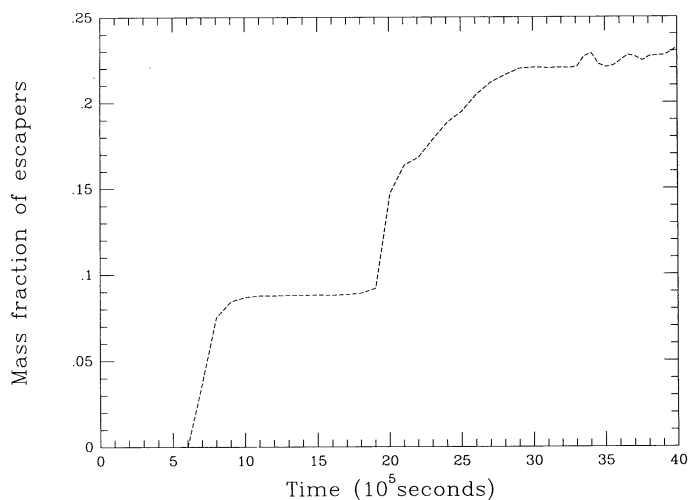


FIG. 12.—Mass fraction of escapers as a function of time for the simulation illustrated in Fig. 10.

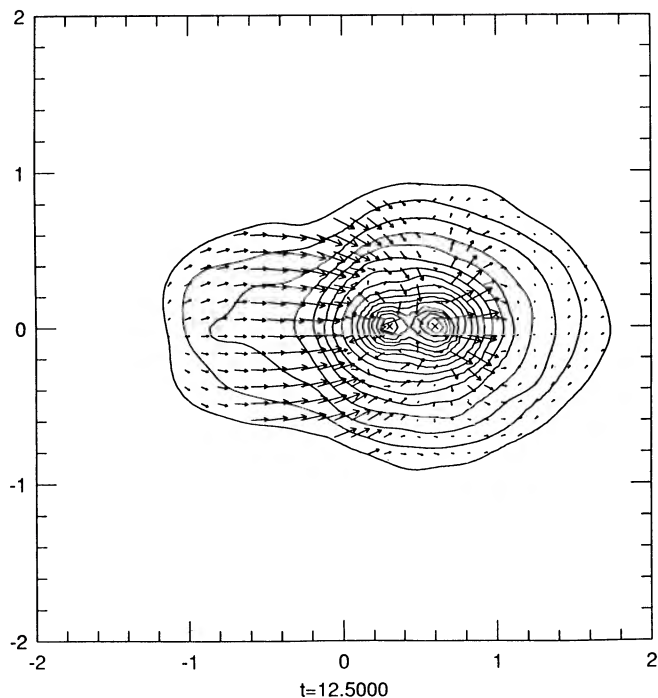


FIG. 13.—Density contour map in a plane perpendicular to that of the initial trajectories, illustrating the common envelope system produced in the simulation illustrated in Fig. 10.

ciently large that the main-sequence star does not fill its Roche lobe, a detached binary system will be formed; we shall call such an outcome “case (i).” Since the main-sequence lifetime for a low-mass star is *extremely* long, it seems unlikely that any further evolution will occur. To produce a detached system, we require $a_f \gtrsim 1 R_\odot$ for $M_{\text{imp}} = 0.4 M_\odot$, and $a_f \gtrsim 1.4 R_\odot$ for $M_{\text{imp}} = 0.6 M_\odot$. The second possible outcome, case (ii), is having the main-sequence star fill its Roche lobe. This will happen when $a_f \lesssim 1.0 R_\odot$ for $M_{\text{imp}} = 0.4 M_\odot$ and when $a_f \lesssim 1.4 R_\odot$ for $M_{\text{imp}} = 0.6 M_\odot$. If the final separation is less than the size of the main-sequence star, then we have our third possible outcome, case (iii), namely, that of a physical merger. Such a merger may occur *before* all of the envelope has been removed; we will thus be left with a rapidly rotating red giant with the main-sequence star enveloping the red giant core. This third case will happen if $a_f \lesssim 0.4 R_\odot$ for $M_{\text{imp}} = 0.4 R_\odot$ and if $a_f \lesssim 0.6 R_\odot$ for $M_{\text{imp}} = 0.6 R_\odot$.

We now use equation (14), for both values of M_{imp} and with a range of values of α , to calculate the initial separation required to produce the three possible outcomes as described above. These are illustrated in Figures 14 and 15. We note that for $\alpha \approx 0.3$ (Livio & Soker 1988; Taam & Bodenheimer 1989), the vast majority of systems produced by a common envelope phase will contain a Roche lobe-filled main-sequence star, i.e., we have case (ii). When the mass of the main-sequence star exceeds that of the white dwarf, mass transfer to the white dwarf will cause the two objects to spiral in toward each other, leading to a second common envelope phase. We also note that in order to produce a large fraction of detached systems, we require $\alpha \gtrsim 0.4$.

5.1.2. White Dwarf Impactor

If the impactor is a white dwarf, we will be left with a white dwarf binary system after the common envelope phase. Such a

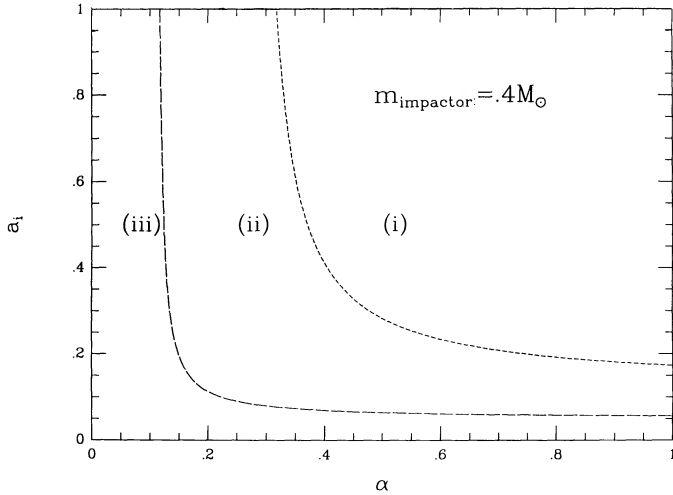


FIG. 14.—Result of a common envelope phase as a function of the initial separation, a_i , and efficiency α for a main-sequence star impactor of mass $M_{\text{imp}} = 0.4 M_{\odot}$. In region (i) a merged system is the product of a common envelope phase. In region (ii) we produce a close binary with the main-sequence star filling its Roche lobe. In region (iii) a detached binary is produced.

system will lose angular momentum through the emission of gravitational radiation on a time scale given by (Landau & Lifshitz 1962)

$$\tau_{\text{GR}} = \frac{5}{32} \frac{c^5}{G^{5/3}} \frac{(M_c + M_{\text{imp}})^{2/3}}{M_c M_{\text{imp}}} \left(\frac{P}{2\pi} \right)^{8/3}, \quad (15)$$

where P is the orbital period of the binary. The two stars will spiral and merge in less than 10^{10} yr if the initial separation satisfies (Iben & Tutukov 1984)

$$\left(\frac{a_f}{R_{\odot}} \right) \lesssim 3.3 \left(\frac{M_c}{M_{\odot}} \right)^{1/4} \left(\frac{M_{\text{imp}}}{M_{\odot}} \right)^{1/4} \left(\frac{M_c + M_{\text{imp}}}{M_{\odot}} \right)^{1/4}. \quad (16)$$

From equation (16) we thus see that $a_f \lesssim 2.1 R_{\odot}$ for $q = 0.75$. Hence, if the efficiency α is appropriately 0.3, all white dwarf binary systems produced in the common envelope phases of binaries formed from encounters between $0.8 M_{\odot}$ red giants and $0.6 M_{\odot}$ white dwarfs will merge in less than 10^{10} yr. Since $M_{\text{imp}} = 0.6 M_{\odot}$ and $M_c \approx 0.32 M_{\odot}$, such mergers will not

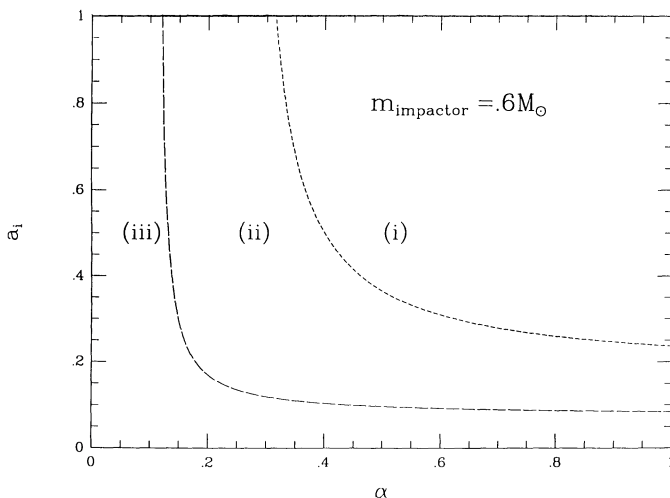


FIG. 15.—As in Fig. 14, but with $M_{\text{imp}} = 0.6 M_{\odot}$

produce Type I supernovae, because the sum of their masses is less than the Chandrasekhar mass. Rather they will produce fairly massive, rapidly rotating white dwarfs. The approximate calculations in § 2 suggest that $\approx 10^2$ such stars will be produced per 10^5 stars in 1 pc^3 in a typical globular cluster core. These rapidly rotating white dwarfs will have a minimum mass $\approx 0.9 M_{\odot}$. To produce a white dwarf of such a mass from a single star requires an initial main-sequence mass $\approx 2.45 M_{\odot}$ (Iben & Renzini 1983). Assuming that our initial stellar population follows the power law $dN \propto M^{-2.5} dM$ and that $0.4 M_{\odot} < M_{\star} < 15.0 M_{\odot}$, we find that the number of primordial white dwarfs with $M_{\text{WD}} \gtrsim 0.9 M_{\odot}$ is ≈ 4000 per 10^5 stars. Hence the relative increase in the number of fairly massive white dwarfs due to collisions will be small. It has also been suggested (Webbink 1984) that a He white dwarf overflowing its Roche lobe and transferring mass onto a CO white dwarf (as will be the case here) may produce an R Coronae Borealis star as helium burning begins in a shell around the CO core, causing the rest of the envelope to expand, producing a very luminous object.

5.2. Common Envelopes Formed in Circularized Systems

We now consider the ultimate fate of bound systems that become circularized rather than having the impactor spiral in to the red giant envelope. In such systems the red giant will eventually overflow its Roche lobe as it expands in its subsequent evolution up the red giant branch, thus producing a common envelope system. Since during this phase of the red giant's evolution only a very small mass fraction of the envelope expands, the binding energy of the red giant will be similar to the value for the initial red giant model. Hence we may still use equation (14) to calculate the final separation of the impactor and the red giant core after the common envelope phase. Because the final separation is relatively independent of the initial separation, the result of a common envelope phase formed in a circularized system will thus be the same as that formed in a close physical collision. Hence we expect to form white dwarf binaries in the case of a white dwarf impactor, and white dwarf/main-sequence star binaries with the latter filling its Roche lobe in the case of a main-sequence star impactor.

5.3. Decay and Spin-up Time Scales

One can compare the decay time scale of the orbit of the impactor and the spin-up time scales of the envelope with the Keplerian time scale of the impactor's orbit within the common envelope. Livio & Soker (1988) define

$$\beta_{\text{CE}} = \frac{\tau_{\text{decay}}}{\tau_{\text{Kep}}}, \quad (17)$$

$$\gamma_{\text{CE}} = \frac{\tau_{\text{spin-up}}}{\tau_{\text{decay}}}. \quad (18)$$

Thus, if $\beta_{\text{CE}} \lesssim 1$, the impactor will spiral in, rapidly depositing energy locally. If $\gamma_{\text{CE}} \lesssim 1$, the spin-up of the envelope will slow down the orbital decay considerably, since the drag force depends on the relative velocity of the impactor with the gaseous envelope. The ratios β_{CE} and γ_{CE} are given by (Livio & Soker 1988)

$$\beta_{\text{CE}} = \frac{\tau_{\text{decay}}}{\tau_{\text{Kep}}} = \frac{F(\mathcal{M})}{12\pi} \left[\frac{M(a) + M_s}{M_s} \right] \left(\frac{V_s}{V_{\text{Kep}}} \right) \left(\frac{\bar{\rho}_a}{\rho_a} \right), \quad (19)$$

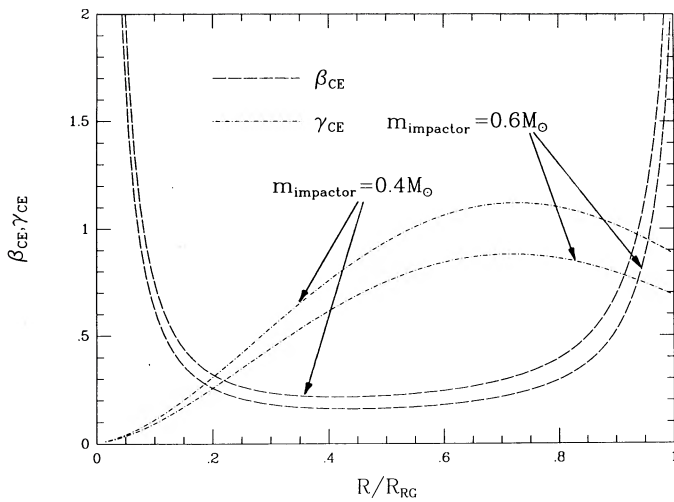


FIG. 16.—Values of $\beta_{CE} = \tau_{Decay}/\tau_{Kep}$ and $\gamma_{CE} = \tau_{spin-up}/\tau_{decay}$ as a function of the fractional radius of the red giant for $M_{imp} = 0.6 M_{\odot}$ and $M_{imp} = 0.4 M_{\odot}$.

where a is the separation, $M(a)$ is the mass in the giant to radius a , ρ_a is the local density in the common envelope, M_s is the impactor mass, V is the relative velocity between the impactor and the common envelope, and $(4\pi/3)\bar{\rho}_a a^3 = M(a)$.

$$\gamma_{CE} = \frac{\tau_{spin-up}}{\tau_{decay}} = 1.2\mathcal{M}^2 \left[\frac{M(a) + M_s}{M_s} \right] \left(\frac{\bar{\rho}_a}{\rho_a} \right) \left(\frac{V_s}{V_{Kep}} \right)^2, \quad (20)$$

where

$$\bar{\rho} = \frac{5}{a^5} \int_{R_{min}}^a r^4 \rho(r) dr.$$

We can now calculate β_{CE} and γ_{CE} for our red giant model for various values of M_{imp} and $V(r)$. In Figure 16 we see β_{CE} and γ_{CE} for $M_{imp} = 0.4 M_{\odot}$ and $M_{imp} = 0.6 M_{\odot}$ assuming $V = V_{Kep}$; this should be compared with Figure 2 in Livio & Soker (1988). We see that in both cases $\beta_{CE} \lesssim 1$ for $0.1 <$

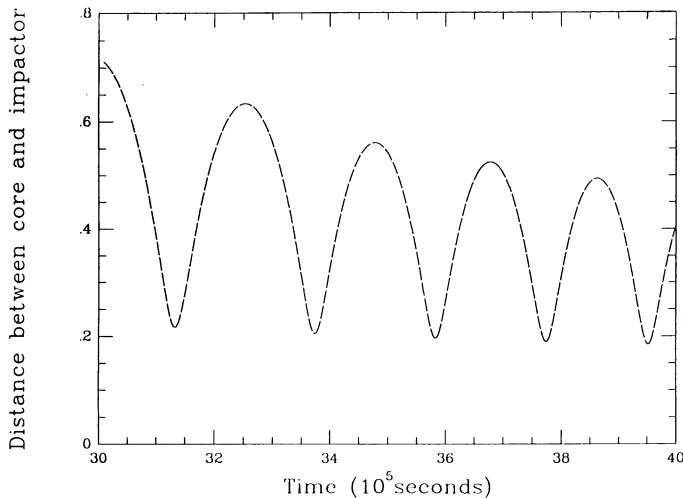


FIG. 17.—Core-impactor separation as a function of time for $M_{imp} = 0.6 M_{\odot}$ and $x_0 = 0.5$.

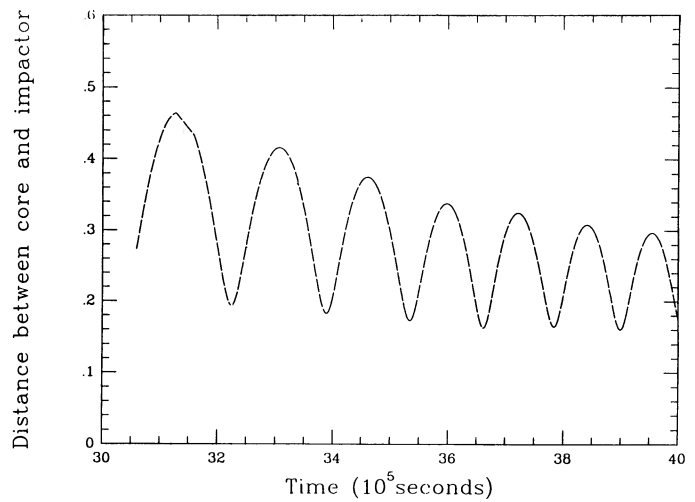


FIG. 18.—As in Fig. 17, but with $M_{imp} = 0.4 M_{\odot}$.

$R/R_{RG} < 0.95$. This suggests that an impactor will rapidly spiral in once at this range of radii. However, it should also be noted that $\gamma_{CE} \lesssim 1$, hence spin-up of the envelope will occur rapidly. This will reduce V and thus the drag force and Mach number, \mathcal{M} . For $\mathcal{M} < 1$, $F(\mathcal{M}) \gg 1$ and β_{CE} will increase. If $\beta_{CE} > 1$, the impactor will dump energy in a torus within the envelope and local effects will become less important.

We can make an estimate of β_{CE} for the two encounters where $x_0 = 0.5$ (colLA.4b and colLA.11a). The distances between the red giant core and the impactor as a function of time for these two simulations are illustrated in Figures 17 and 18. From this figure we can make an estimate of β_{CE} by measuring the shift in core-impactor separation between successive maxima, Δa . Hence $\tau_{decay} \approx (a/\Delta a)\Delta t$, where Δt is the time between two successive maxima $\equiv \tau_{Kep}$. Hence we have $\beta_{CE} = (a/\Delta a)$. The values for β_{CE} calculated in this way are given in Table 5. We see that the measured values of β_{CE} always greatly exceed the theoretical values calculated assuming $V = V_{Kep}$. This is because we have spun up the envelope of the red giant, thus reducing the Mach number of the flow, \mathcal{M} , to below unity, thus giving $F(\mathcal{M}) \gg 1$ and greatly increasing β_{CE} . A more detailed study of the common envelope process and the calculation of the parameters α , β_{CE} , and γ_{CE} will follow in a later paper.

5.4. Can We Distinguish a Binary Formed by Capture from a Primordial One?

We now consider whether one could distinguish observationally between binary systems formed from close encounters

TABLE 5
COMMON ENVELOPE EVOLUTION

| Collision | Time (10 ⁵ s) | Separation ^a /R _{RG} | β_{CE} |
|-----------------|--------------------------|--|--------------|
| CoILA.11a | 34.61 | 0.374 | 9.67 |
| CoILA.11a | 35.98 | 0.338 | 14.05 |
| CoILA.11a | 37.23 | 0.325 | 21.68 |
| CoILA.11a | 38.41 | 0.308 | 22.45 |
| CoILA.4b | 34.78 | 0.561 | 10.65 |
| CoILA.4b | 36.78 | 0.524 | 15.75 |

^a Separation between red giant core and point mass impactor.

and primordial systems. We consider the case of a $0.6 M_{\odot}$ white dwarf in a circular orbit, of radius $R_{\text{orb}} = 80 R_{\odot}$. Let us try to produce an identical system, beginning with a binary system of two main-sequence stars. The primary will expand as it becomes a red giant, filling its Roche lobe, resulting in a common envelope phase. The gaseous envelope of the primary will be removed, leaving a white dwarf behind, orbiting the intact secondary. If the white dwarf has a mass $\simeq 0.6 M_{\odot}$, as assumed here, the initial primary mass is required to be $\simeq 1.1 M_{\odot}$. We may calculate the *maximum* final separation of the two stars after this first common envelope stage by setting $a_i = \infty$ in equation (14). We thus obtain

$$a_{f\text{max}} \simeq \frac{\alpha G M_c M_{\text{imp}}}{2E_{\text{env}}}. \quad (21)$$

If we assume $E_{\text{env}} \propto M_{\text{env}}(M_{\text{env}} + M_c)$, then the binding energy of the $1.1 M_{\odot}$ red giant envelope will be approximately double that of the $0.8 M_{\odot}$ red giant. Inserting suitable values for M_c , M_{imp} , and E_{env} into the above equation, we thus obtain

$$a_{f\text{max}} \simeq 7.0\alpha R_{\odot}; \quad (22)$$

hence we conclude that it is *extremely* difficult to produce the desired binary from a primordial binary, since we would need some mechanism to give $\alpha \gtrsim 10$.

6. CONCLUSION

We have successfully simulated encounters between a $0.8 M_{\odot}$ red giant and a $0.6 M_{\odot}$ white dwarf and between the red giant and 0.4 and $0.6 M_{\odot}$ main-sequence stars; such encounters are applicable to globular cluster cores where the turnoff mass is observed to be $\simeq 0.8 M_{\odot}$. We see a fractional mass loss larger than that observed in previous simulations of collisions

between main-sequence stars. We have shown that impactors passing within $\simeq 2R_{\text{RG}}$ will become bound to the red giant, resulting in either the production of a binary engulfed in a common envelope of gas or a close binary system. In the case of a white dwarf impactor, it seems *extremely* difficult to produce a similar close binary system from a primordial binary system. Simple calculations suggest that a common envelope phase will produce a white dwarf binary of separation $\sim 2-3 R_{\odot}$ or less when the impactor is a low-mass white dwarf. If the impactor is a low-mass main-sequence star, the nature of the final object is a function of the initial impact parameter and efficiency α . For extremely close physical collisions, a rapidly rotating red giant seems likely to be produced, as the main-sequence star impactor spirals in and merges with the red giant core. The most probable outcome for most encounters appears to be the production of a close white dwarf/main-sequence binary, with the latter filling its Roche lobe. If the main-sequence star is more massive than the white dwarf, mass transfer onto the white dwarf will produce a second common envelope phase. More studies of the evolution of common envelope systems will be carried out, so that one may compare numerical results with the theory described by Livio and Soker.

We would like to thank Marc Herant and Julio Navarro for many useful discussions. We would also like to thank Al Cameron for the use of the computer hardware that made these simulations possible. M. B. D. would like to thank the Theoretical Astrophysics Group, T-6, and IGPP at Los Alamos National Laboratory for a graduate student assistantship during the past two summers. W. B. acknowledges partial support from the Swiss National Science Foundation.

REFERENCES

- Bailyn, C. D. 1988, *Nature*, 332, 330
 Bailyn, C. D., Grindlay, J. E., & Garcia, M. R. 1990, *ApJ*, 357, L35
 Begelman, M. C., & Rees, M. J. 1978, *MNRAS*, 185, 847
 Benz, W. 1990, in *Numerical Modeling of Stellar Pulsation: Problems and Prospects*, ed. J. R. Buchler (Dordrecht: Kluwer), 269
 Benz, W., & Hills, J. G. 1987, *ApJ*, 323, 614
 Benz, W., Hills, J. G., & Thielemann, F. K. 1989, *ApJ*, 342, 986
 de Kool, M. 1990, *ApJ*, 358, 189
 Durisen, R. H., & Tohline, J. E. 1985, in *Protostars and Planets II*, ed. D. C. Black & M. S. Shapley (Tucson: Univ. Arizona Press), 534
 Eggleton, P. P. 1983, *ApJ*, 268, 368
 Fabian, A., Pringle, J., & Rees, M. J. 1975, *MNRAS*, 172, 15P
 Goodman, J., & Hernquist, L. 1991, *ApJ*, submitted
 Hills, J. G. 1975, *Nature*, 254, 295
 ———. 1978, *MNRAS*, 182, 517
 Hills, J. G., & Day, C. A. 1976, *Ap. Letters*, 17, 87
 Iben, I., & Renzini, A. 1983, *ARA&A*, 21, 271
 Iben, I., & Tutukov, A. V. 1984, *ApJS*, 54, 335
 Landau, L., & Lifshitz, E. 1962, *Quantum Mechanics* (London: Wiley)
 Livio, M., & Soker, N. 1988, *ApJ*, 329, 764
 Livne, E., & Tuchman, Y. 1988, *ApJ*, 332, 271
 McMillan, S. L., Taam, R. E., & McDermott, P. N. 1990, *ApJ*, 354, 190
 Mengel, J. G., Sweigart, A. V., & Demarque, P. 1979, *ApJ*, 40, 733
 Rasio, F. A., & Shapiro, S. L. 1990, *ApJ*, 354, 201
 ———. 1991, *ApJ*, submitted
 Shapiro, S. L., & Teukolsky, S. A. 1983, in *Black Holes, White Dwarfs and Neutron Stars* (New York: Wiley), 173
 Taam, R. E., & Bodenheimer, P. 1989, *ApJ*, 337, 849
 Webbink, R. F. 1984, *ApJ*, 277, 355
 Zahn, J.-P. 1989, *A&A*, 220, 112